1 **A multi-level investigation on the mechanical response of TRM-strengthened masonry**

2

3 Ali Dalalbashi[1], Bahman Ghiassi[2], Daniel V. Oliveira[3]

4

5 ABSTRACT

6 This paper presents a multi-level experimental and analytical investigation on the mechanical

7 performance of TRM composites used for strengthening existing masonry structures. Micro

8 (fabric-to-mortar bond), meso (TRM-to-substrate bond), and macro (TRM tensile response and in-

9 plane and the out-of-plane response of TRM-strengthened masonry) response of TRMs are

10 combined and investigated in-depth for this reason. These results help to understand the

11 mechanisms controlling the response of these composites and their performance at the structural

12 scale.

13

14 Keywords: *TRM; FRCM; TRM-strengthened masonry; in-plane behavior; out-of-plane behavior,*

15 *multi-level experimental testing.*

16

[1] PhD Student, ISISE, Department of Civil Engineering, University of Minho, Guimarães, Portugal. E-mail: alidalalbashi@gmail.com. https://orcid.org/0000-0003-0486-1433

[2] Assistant Professor, Centre for Structural Engineering and Information, Faculty of Engineering, University of Nottingham, Nottingham, United Kingdom. E-mail: bahman.ghiassi@nottingham.ac.uk. http://orcid.org/0000-0003-4212-8961

[3] Associate Professor, ISISE, Department of Civil Engineering, University of Minho, Guimarães, Portugal. E-mail: danvco@civil.uminho.pt. http://orcid.org/0000-0002-8547-3805

1 Introduction

Many unreinforced masonry (URM) structures are prone to catastrophic failure during earthquakes [1, 2] due to their weakness against in-plane and out-of-plane seismic loads [3]. The development of strategies for repairing and strengthening structures made of these materials has been the object of many studies during the last decades. Among these, externally bonded reinforcement is one of the most common strengthening methodologies, in which a composite material is attached to the external surface of weak structural components. Traditionally, Fiber Reinforced Polymers (FRPs) were mainly used as the strengthening material in this system. However, the issues related to sustainability, durability, poor performance at high temperatures, and compatibility of these composites with masonry indicated the need to use and develop novel repair materials. In an attempt to alleviate the drawbacks that arise from the use of FRPs [4, 5], Textile Reinforced Mortar (TRM) composites have been proposed in the last years [6, 7].

TRMs are composed of continuous yarns/fibers embedded in an inorganic matrix and present several advantages: they have a high thermal capacity, are applicable to wet surfaces, are removable, and can be compatible with masonry and concrete surfaces [4, 8]. The large variety of available fabric types and mortars allows TRM composites to develop with an extensive range of mechanical properties [9, 10]. When properly designed, TRMs show a pseudo-ductile response with distributed cracking, which makes them interesting for seismic strengthening applications [11, 12].

Despite the recent attention these composites have found as a suitable strengthening material, many issues regarding the mechanical response and durability of these composites are still unknown. Recent studies have mainly focused on the tensile response of TRMs and the bond of TRM-to-masonry. Studies at the structural scale [13–15] or the composite scale [16–19] can also be found. However, comprehensive experimental/analytical studies from materials to structural scale are still missing [20, 21]. Structural scale tests (diagonal tension or out-of-plane tests on TRM-strengthened masonry) are still few and mainly focused on the effect of textile and substrate types [22, 23], the number of textile layers [24], and symmetrical or asymmetrical application of the repair [13, 25, 26]. Nevertheless, there is a lack of understanding of the parameters controlling the response at the structural scale. This understanding will be developed in this paper through a comprehensive experimental and analytical study from materials to structural scale.

2   Experimental program

The experimental campaign consisted of materials mechanical characterization tests, textile-to-mortar pull-out tests, TRM-to-substrate bond tests, TRM direct tensile tests, and finally, diagonal compression and flexural tests on TRM-strengthened masonry panels. The role of sandblasting on the masonry surface is also investigated. A detailed description of the materials, preparation of specimens, and the test methods are presented in this section and Online Resource 1. The timeline used for the samples' preparation and testing is presented in Fig. 1 to facilitate understanding of the sequences and the considered framework.

2.1   Materials

Solid clay bricks ($200 \times 100 \times 50$ mm^3) were used to construct the masonry wallets and the single-lap shear specimens. Two different lime-based mortars were used in this study, referred to as M1 and M2. Mortar M1 is a high-ductility hydraulic mortar and is commercialized as a TRM matrix (Planitop HDM Restauro). This two-component mortar was prepared by mixing the powder and liquid in a low-speed mechanical mixer to form a homogeneous paste. Mortar M2 utilized to build the masonry wallets is also based on lime and ecopozzolan (Mape-Antique MC). The TRM composite used here is a glass-based TRM. The glass fabric was a woven biaxial fabric mesh made of alkali-resistance fiber glass (Mapegrid G220). Its mesh size and area per unit length are equal to 25×25 mm^2 and 35.27 mm^2/ m, respectively.

2.2   Material characterization tests

The compressive and flexural strength of the mortars was tested according to ASTM C109 [27] and EN 1015-11 [28]. Five cubes ($50 \times 50 \times 50$ mm^3) and five prismatic ($40 \times 40 \times 160$ mm^3) specimens were prepared for each mortar. The mortar M1 strength was measured after 28 and 90 days, while the mortar M2 strength was tested after 28 and 120 days (see also Fig. 1). Elastic modulus and splitting tensile strength of the mortars were assessed according to EN 12390-13 [29] and ASTM C496 [30]. Five cylinders with 70 mm diameter and 150 mm in length were made for each test, totaling ten specimens for each mortar type. Mortar samples were demolded after three days and placed in a damp environment for seven days; then, samples were cured in the lab environmental conditions (20°C, 67% RH) until testing.

The brick's compressive strength was characterized according to ASTM C67 [31] and EN 772-1 [32] and along with all directions, i.e., flatwise, lengthwise, and widthwise directions. For each

3

1   direction, five cubes (40×40×40 mm^3) were used. Flexural strength and elastic modulus of the

2   brick were calculated according to EN 1015-11 [28] and EN 12390-13 [29], respectively, by using

3   five prismatic specimens (40×40×160 mm^3) for each test. For measuring the flexural strength, the

4   load was applied perpendicular to the flatwise and lengthwise surface of the brick; while, the elastic

5   modulus was measured along the lengthwise direction only.

6   The compressive and the flexural tests were performed using a Lloyd testing machine under force-

7   controlled conditions at a rate of 150 N/s and 10 N/s, respectively. In the compressive tests, a pair

8   of Teflon sheets with a layer of oil between them was placed between the specimen and the

9   compression plates to reduce the possible friction effect. For measuring the elastic modulus, a

10   universal testing machine (load capacity of 100 kN) and LVDTs (3 for cylinder and 4 for prismatic

11   specimens) with a 5 mm range and 1-µm sensitivity were used. Tensile splitting tests were also

12   performed using the universal testing machine and introducing monotonic displacements at a rate

13   of 0.12 mm/min.

14   The compressive strength of masonry prisms was obtained according to ASTM C1414 [33] by

15   conducting the tests on prisms made of three bricks and M2 bed joint mortar about 20 mm thick.

16   These tests were performed at 28 and 120 days (five specimens at each age). A universal testing

17   machine with a load capacity of 1000 kN under displacement-controlled conditions (0.3 mm/min)

18   was used to apply the load perpendicular to the flatwise direction of bricks. Additionally, the shear

19   strength of five triple-brick prisms was investigated at 28 days of age based on EN 1052-3 [34].

20   Before applying the shear load, the pre-compression load was applied to the specimens. A

21   universal testing machine (load capacity of 100 kN) under displacement-controlled conditions

22   (0.3 mm/min) was used to apply the load parallel to the bricks' lengthwise direction.

23   The tensile strength and elastic modulus of the fabrics in both warp and weft directions were

24   measured through direct tensile tests on single yarns. A universal testing machine (load capacity

25   of 10 kN) was used for this purpose. The tests were performed on five specimens with a free length

26   of 300 mm under displacement-controlled conditions (0.3 mm/min). A 100 mm clip gauge, which

27   was located at the center of the specimen, and the internal LVDT of the machine measure the yarn

28   deformation.

1   2.3   Pull-out test

2   The single-sided pull-out test setup developed in [35] was used for studying the bond behavior

3   between the yarn and the mortar. The specimens were prepared by embedding single yarns in a

4   disk-shaped mortar with a cross-section of 125×16 mm^2 for 50 and 100 mm (Fig. 2a). Before this,

5   the free end of the yarn was covered with an epoxy resin block with a rectangular cross-sectional

6   area of 10×16 mm^2 and 200 mm long [35]. Specimens were demolded after three days of

7   preparation and covered by wet clothes and plastic for seven days. Those were then placed in the

8   lab environmental conditions (20°C, 67% RH) and tested after 90 days of age. Five samples were

9   prepared and tested under the pull-out testing scheme in total.

10 The test setup consisted of U-shape steel supports attached to a rigid frame to fix the samples (Fig.

11 2a). The tests were performed using a servo-hydraulic system with a maximum capacity of 25 kN

12 and a mechanical clamp that pull the epoxy resin from the top. In another study conducted by the

13 authors [36], displacement rate effects on the pull-out response of glass-based TRM were

14 investigated. The results illustrated that the bond behavior did not show any considerable changes

15 by increasing the rate from 0.3 mm/min to 1.0 mm/min. Hence, to save time, the pull-out test's

16 displacement rate of 1.0 mm/min was adopted in this study. Three LVDTs recorded the slip with

17 a 20 mm range and 2-µm sensitivity, as shown in Fig. 2a. The mean values of these LVDT

18 measurements are presented as the slip in the experimental results.

19 2.4   TRM tensile test

20 Five prismatic ($550 \times 70 \times 10$ mm^3) specimens were prepared for performing direct tensile tests, as

21 shown in Fig. 2b. The fabric mesh consisted of three warp and thirteen weft glass yarns, in which

22 the warp yarns were parallel to the tensile load direction. The samples included a 100 mm free

23 yarn length at each side and a 350 mm central region in which the fabrics were embedded in the

24 mortar (Fig. 2b). The curing conditions of these samples were similar to the pull-out test

25 specimens.

26 One week before the tests, two steel plates ($100 \times 75 \times 10$ mm^3) were attached to the free part of

27 yarns after saturating it with resin to avoid rupture of the clamping fabric area during the tests.

28 Two mechanical clamps gripped the samples, and two LVDTs with a 20 mm range and 2-µm

29 sensitivity were placed at both sides of the tensile specimen to record the deformation, as illustrated

30 in Fig. 2b. A servo-hydraulic jack with a maximum capacity of 25 kN applied the direct tensile

5

1   load to the specimens through the clamps under a displacement control rate of 0.3 mm/min. The

2   results are presented in terms of stress-strain curves in section 3.3. The stress introduced to the

3   samples was calculated considering the cross-section area of the yarns. Simultaneously, the strain

4   was computed by dividing the mean value of the displacements recorded from the two LVDTs by

5   their base length (310 mm).

6   ## 2.5   Single-lap shear test

7   Single-lap shear specimens were prepared by applying the TRM composite to the bricks flatwise

8   surfaces. Two groups of samples were prepared with 100 mm bonded length. In one group, the

9   original brick surface was used (method a), while in the second group, the brick surface was

10   sandblasted to increase the surface roughness, here termed method b [37]. Besides, to investigate

11   the effect of bond length, an additional embedded length of 150 mm was utilized with sandblasted

12   bricks (method b). Before applying the TRM composite, the bricks were pre-wetted for one hour

13   to ensure a semi-saturated condition. The width and the total thickness of TRM were equal to

14   70 mm and 10 mm, respectively, as shown in Fig. 2c. The embedded glass mesh included three

15   warp yarns, three transverse elements for 100 mm, and five transverse elements for 150 mm bond

16   length, while the free length of the fabrics was 250 mm. For each type of brick surface and

17   embedded length, five specimens were constructed and named as SL100-a for the original brick

18   and SL100-b and SL150-b for single-lap shear specimens constructed with the sandblasted brick.

19   The curing condition of these samples was similar to the pull-out test specimens.

20   For performing the tests, two aluminum plates ($65\times65\times2$ mm^3) were glued to the extremity of the

21   yarns after saturating yarns with resin seven days before testing to facilitate the gripping and ensure

22   a uniform load transfer. A stiff supporting frame and two clamps supported the specimens, as

23   shown in Fig. 2c. Two LVDTs with a 20 mm range and 2-µm sensitivity were placed at the loaded

24   end to measure the slip during the tests. A servo-hydraulic jack with a maximum load capacity of

25   50 kN was used to perform the single-lap shear tests at a displacement rate of 0.3 mm/min. A

26   preload equal to 100 N was applied to specimens before testing to facilitate the LVDTs attachment

27   [38].

28   ## 2.6   Masonry wallets

29   Solid clay brick and mortar M2 were used to build the masonry wallets. Again, to investigate the

30   brick surface preparation effect on the structural performance of TRM-strengthened masonry, two

6

1 groups of samples were prepared: in one group, original bricks were used, while in the second

2 group, sandblasted bricks were used (lengthwise direction) to build the wallets. Similar to single-

3 lap shear specimens, bricks were immersed in water for one hour before being used. Thirty days

4 after constructing and curing wallets in lab environmental conditions (20°C, 67% RH), TRM

5 composites were applied (with 10 mm thickness mortar), and wallets were stored in the lab for 90

6 additional days. The wallets strengthened with TRM composites were cured under wet clothes and

7 plastic during the first week, similar to the procedure considered for the pull-out and single-lap

8 shear tests.

9 *2.6.1   Diagonal compression tests*

10 According to ASTM E519 [39], diagonal compression tests were performed on masonry wallets

11 with dimensions of $540 \times 540 \times 100$ mm^3, as shown in Fig. 3a. Nine wallets were constructed so that

12 three of them were unreinforced masonry panels (named IU), while six others were strengthened

13 by one layer of glass-based TRM composite applied on both faces. Three out of the six

14 strengthened panels were made with the original bricks (named ISa), and the other three with the

15 sandblasted bricks (named ISb). A servo-hydraulic system with a maximum capacity of 300 kN

16 was used for performing these tests at a displacement rate of 0.3 mm/min. The load was applied

17 through steel shoes ($115 \times 115 \times 15$ mm^3) placed at diagonally opposing bottom and top corners of

18 the wallets [15]. As shown in Fig. 3a, two 20 mm range and 2-μm sensitivity LVDTs measure the

19 vertical and horizontal deformation of the wallets during the tests.

20 *2.6.2   Out-of-plane tests*

21 Flexural tests were performed promoting preferential damage and failure either parallel or normal

22 (perpendicular) to bed joints and according to EN 1052-2 [40]. Nine specimens were prepared for

23 each direction. Therefore, three wallets were un-strengthened, and six (3 sandblasted and 3

24 original) were strengthened with TRM only at one side of the wallets (opposite side of the loading).

25 Dimensions of the out-of-plane wallets failure parallel and normal to bed joints were

26 $540 \times 420 \times 100$ mm^3 and $520 \times 330 \times 100$ mm^3, respectively, as shown in Fig. 3b and Fig. 3c. Based

27 on EN 1052-2 [40], for wallets where failure occurs parallel to bed joint, a minimum of two-bed

28 joints should be within the inner support (constant moment length), see Fig. 3b. However, for

29 failure occurring normal to bed joint, a minimum of one head joint must be within the inner support

30 (Fig. 3c). The fabric mesh was placed so that the warp yarns were parallel to the longitudinal axis

31 of specimens. In total, there were 17 and 12 warp yarns in the out-of-plane wallets failure parallel

7

1   and normal to bed joints, respectively. Meanwhile, 21 weft yarns were in both types of flexural

2   wallets.

3   Specimens were tested in a vertical configuration (to omit the effect of specimens' self-weight on

4   the results) under four-point bending so that the strengthened face was subjected to tension. The

5   distance between the outer and inner bearings was 420 mm and 170 mm, respectively. Four

6   LVDTs were used with a 20 mm range and 2-μm sensitivity to measure the sample deformation at

7   the middle and the location of inner bearings, as shown in Fig. 3b and Fig. 3c. The tests were

8   performed at a displacement rate of 0.3 mm/min and with a servo-hydraulic jack with a maximum

9   load capacity of 50 kN.

10   These specimens are named XYZ, in which X is related to the type of out-of-plane failure (P or

11   N), Y represents the existence of un-reinforced (U) or strengthened (S), and Z is linked to the brick

12   surface "a" for original brick, and "b" for sandblasted brick. For example, wallet NSa is an out-of-

13   plane wallet failure normal to the bed joints, strengthened and constructed by the sandblasted

14   bricks.

15   3   Results and discussion

16   3.1   Material characterization results

17   Table 1 presents the mean strength of the mortars and the brick. It can be observed that by

18   increasing the mortar age, the compressive strength of both mortars M1 and M2 increases by 40%

19   and 64%, respectively, from 28 to 90 days. A similar increase is observed for the splitting tensile

20   strength (56% and 67%, respectively for mortar M1 and mortar M2), while the flexural and elastic

21   modulus do not show any considerable change. This observation recalls that the maximum strength

22   of the utilized lime-based mortars does not reach its peak value after 28 days, as opposed to

23   cementitious mortars [41]. In another study conducted by authors [36], the compressive strength

24   of mortar M1, which was cured only one day under plastic and then stored in the environmental

25   lab (20°C and 60% RH), reached 7.07 MPa and 7.84 MPa for 28 and 90 days, respectively. These

26   values are 12.0 MPa and 16.8 MPa in this work, being 1.7 and 2.1 times that of the previous study.

27   This difference is due to more appropriate curing conditions considered in this study (covered by

28   wet clothes and plastic for seven days and then stored in a 20°C and 67% RH environmental lab).

29   The brick compressive strength is different in each direction owing to its anisotropic properties, as

30   reported in Table 1. Meanwhile, the flexural strength of the clay brick is almost equal in flatwise

8

1 and lengthwise directions. Additionally, the mean compressive strength of the masonry prism after

2 28 days is equal to 10.9 MPa with a coefficient of variation (CoV) of 8 %. This value for the 120

3 days age is 11.1 MPa (CoV=8 %). Although the compressive strength of the mortar M2increases

4 considerably, it does not significantly affect the compressive strength of the prism. The shear

5 strength of masonry prisms at 28 days is equal to 0.26 MPa (CoV=18 %).

6 The average tensile strength, Young's modulus, and rupture strain of the warp glass yarn are

7 875 MPa (CoV=13 %), 65.94 GPa (CoV=5 %), and 1.77 % (CoV=10 %), respectively. These

8 values for the weft direction are 685 MPa (9 %), 69.87 GPa (4 %), and 1.45 % (11 %),

9 respectively. This observation shows that the tensile strength of the weft glass yarn is less than the

10 warp yarn by 78%, and one should consider when analyzing the behavior of TRM-strength

11 masonry panels.

12 ## 3.2 Pull-out response

13 Fig. 4 shows the load-slip curves of the single glass yarn-based TRM for 50 and 100 mm bond

14 length. As shown in Fig. 4, the load-slip curves of the specimens with 50 mm and 100 mm

15 embedded lengths are different, which is due to the differences in their failure modes. For 100 mm

16 embedded length, yarn rupture occurs after reaching the full strength of the yarns (as shown in Fig.

17 4b). This observation shows that a 100 mm embedded length is longer than the effective bond

18 length, which is in line with [42]. The mean values of the main characteristics of the pull-out

19 response are summarized in Table 2, which are the peak load (P_P) and its corresponding slip (S),

20 debonding and pull-out energy ($E_{deb.}$, $E_{pull.}$), and initial stiffness according to [42]. Additionally,

21 the bond-slip law parameters for 50 mm embedded length are presented in Table 2, including pull-

22 out bond shear strength (τ_{max}), frictional shear strength (τ_f), bond modulus (κ), and slip-hardening

23 coefficient (β). For calculating these parameters, the reader is referred to [35]. In the next sections,

24 τ_f will be used to predict the crack spacing in tensile tests. For the purpose of determining bond

25 parameters (e.g., τ_{max}, τ_f), the slip between the yarns and the mortar is considered a fundamental

26 property and these values cannot be obtained if the failure mode is rupture of the fiber. Presentation

27 of the bond-slip law parameters when rupture of the fibers occurs is also not physically justifiable.

28 ## 3.3 TRM tensile behavior

29 The tensile response of the tested composites is shown in Fig. 5. All the samples failed by rupture

30 of the yarns implying the adequacy of the clamping system used. The crack patterns developed in

9

1 the samples are also shown in Fig. 5. On average, three cracks with an average distance of 101 mm

2 are formed on the samples (Table 2). This crack spacing indicates that the pull-out test results

3 obtained from samples with 50 mm embedded length need to be used to interpret the bond effects

4 on the post-cracking response of these composites.

5 The main characteristics average value of the tensile response of specimens are also obtained and

6 presented in Table 2 in terms of elastic modulus (E_1, E_2, E_3), strain (ε_1, ε_2, ε_3), and stress (σ_1, σ_2,

7 σ_3) corresponding to the linear stage, crack development stage, and post-cracking stage [41]. The

8 mean value of the maximum tensile stress is equal to 995.6 MPa that is slightly higher than the

9 tensile strength of the single yarns. This observation shows the stress has been distributed

10 uniformly among the yarns, and the composite action has also slightly enhanced the final tensile

11 response of the TRM system.

12 Comparing these results with the ones previously presented by the authors in [41] (where a

13 different curing regime was followed: i.e., the specimens were cured for one day under plastic and

14 then stored in the environmental lab for 90 days and therefore) shows the importance of curing

15 conditions on the mechanical response of these composites (the results presents in this paper are

16 around 1.6 times higher for the cracking strength and 5.6 times for the elastic modulus).

17 Meanwhile, the saturated cracking distance is 1.58 times larger in the present study due to higher

18 bond strength in samples cured under better conditions.

19 3.4   TRM-to-substrate bond behavior

20 A comparison among the results of SL100-a, SL100-b, and SL150-b specimens clearly shows the

21 effect of sandblasting on the TRM-to-substrate bond behavior, see Fig. 6. The failure mode of the

22 SL100-a samples is the delamination of the TRM from the substrate, while yarns slippage,

23 followed by tensile rupture, is observed in the SL100-b samples. Additionally, in SL150-b

24 specimens, all yarns ruptured by reaching the maximum load. The load-slip curves are also

25 consequently different in these three sets of samples.

26 The main experimental parameters, such as the peak load (P_P) and its corresponding slip (s), the

27 fabric stress (σ), and the initial stiffness (K) are obtained for the tested samples and presented in

28 Table 2. σ is calculated by dividing the peak load by the cross-section area of the yarns (2.65 mm^2).

29 Since the bond length in the TRM systems considered here is long, the assumption of a uniform

30 distribution of shear stresses along the bond length is erroneous. Also, the definition of the bond

10

1   strength in single-lap shear tests can only be considered if the failure mode is consistent (always

2   slippage of the yarns from the mortar or detachment of the mortar from the substrate) and therefore

3   can be misleading in the analysis of these tests.

4   It can be seen that sandblasting has a significant effect as SL100-b samples show a peak load and

5   a corresponding slip around 2.14 times higher than those of SL100-a. Also, the initial stiffness of

6   SL100-b specimens is 2.12 times higher than the SL100-a samples. As expected, by increasing the

7   embedded length, the peak load and its corresponding slip increase by 44% and 33% in SL150-b

8   specimens compared to SL100-b specimens. The initial stiffness of SL150-b, however, decreases

9   by 45%.

10   The average fabric stress (σ) of SL100-b specimens is 575.4 MPa (see Table 2), which is very

11   close to the stress corresponding to first mortar cracking in tensile tests (567.5 MPa). This

12   observation shows that before the formation of any cracks in the mortar, complete debonding

13   occurs in those samples leading to a substantial decrease in the bond strength of the whole system.

14   On the other hand, the average value of σ in SL150-b specimens is 827.8 MPa, almost equal to the

15   glass yarn strength (875 MPa). This high level of utilization of the strengthening system is due to

16   the combined effect of embedded length and surface preparation. Comparison of the load-slip

17   curves obtained from the pull-out and single-lap tests, see Fig. 6b, shows that a higher peak load

18   and initial stiffness are obtained from the pull-out tests performed on samples with similar

19   embedded lengths (e.g., 100 mm bond length, see Table 2). This difference shows that even when

20   the TRM-to-substrate bond has high quality, there can be a significant difference between the pull-

21   out and single-lap results due to differences in the boundary conditions and stress distribution in

22   these two types of specimens.

23   3.5   Diagonal compression test results

24   The load-displacement (vertical and horizontal LVDT measurements) response of the unreinforced

25   and strengthen panels are presented in Fig. 7a. The curves are calculated by the average of axial

26   or transversal LVDTs. The effect of strengthening on the strength of the masonry wallets is

27   considerable, see Table 3. The strengthened panels show increases of 3.07 and 3.70 in the peak

28   load in ISa and ISb wallets, respectively, compared to IU specimens. Also, sandblasting of the

29   surface (in ISb) has led to a 19.8 % increment of the shear strength (compared to ISa wallets).

11

1   As for the IU panels, the failure is brittle and composed of sliding along the mortar joint and

2   cracking in masonry units with no considerable crack development before failure (see cracking

3   pattern at failure in Fig. 7b). In ISb wallets, two vertical cracks occur initially in the central region

4   of the TRM composite, followed by tensile rupture of the yarns and further development of axial

5   cracks. The distance between the cracks varied from 35 to 100 mm, similar to the crack spacing

6   observed in tensile tests. This observation shows a little difference in ISa specimens, in which the

7   TRM composite partially debonded from the masonry substrate before reaching the maximum

8   load.

9   The shear stress (τ') and strain (γ) in the center of the panel can be calculated according to

10   ASTM- E 519-2 [39]. The shear stress (τ') can be obtained as:

11    $$\tau' = \frac{P\cos\theta}{A_n} \quad\quad\quad\quad (1)$$

12   P and θ are the applied load and the angle between the bed joint and the main diagonal of the

13   wallet, respectively. A_n, which is equal to 5400 mm^2, is the net area of the specimen calculated as

14   follows:

15    $$A_n = \left(\frac{L+H_w}{2}\right) t.n' \quad\quad\quad\quad (2)$$

16   where L, H_w, and t are the length, the height, and the thickness of the panel, respectively, and are

17   equal to 540 mm, 540 mm, and 100 mm. n' is the percentage of the gross area of the unit that is

18   solid, expressed as a decimal. The shear strain (γ) is calculated as follows:

19    $$\gamma = \frac{\Delta_v + \Delta_h}{g} \quad\quad\quad\quad (3)$$

20   Δ_v, Δ_h, and g are the axial shortening, the transversal extension, and the axial gauge length,

21   respectively.

22   The average shear stress-strain curves of each series, obtained from the above formulations, are

23   plotted in Fig. 7b. In addition, Table 3 reports the maximum shear stress (τ'_{max}) and its

24   corresponding strain (γ_{max}), as well as the pseudo-ductility ratio ($\mu_{diagonal} = \gamma_u / \gamma_y$) and the shear

25   modulus (G) of each specimen, which are the main parameters characterizing the shear behavior

26   of the masonry wallets [17]. In this study, γ_u is the ultimate shear strain corresponding to a 20 %

27   strength drop on the post-peak softening branch of the shear stress-strain curve [15, 17, 43, 44].

28   Also, γ_y is introduced as the shear strain at 75 % of the maximum shear stress [13, 14, 17, 45].

12

1 Since the IU specimens only bear load until the peak point, γ_u is considered equal to γ_{max} to

2 calculate the pseudo-ductility ratio. Furthermore, G is defined as the secant modulus between 5%

3 and 30% of the maximum shear stress [22, 46].

4 A comparison between the IU and the strengthened wallets (ISa and ISb) illustrates that

5 strengthening with TRM composite leads to a significant increment of all the parameters

6 mentioned above, as shown in Table 3, which is also in line with previous studies [14, 15, 19, 26].

7 Sandblasting of the masonry surface seems to have a significant effect on controlling the failure

8 mode and, consequently, the mechanical performance of the strengthened wallets. From Table 3,

9 τ'_{max}, γ_{max}, and μ of the ISb panels are 1.24, 1.22, and 1.26 times higher than for ISa wallets,

10 respectively; however, sandblasting does not seem to have a significant influence on the shear

11 modulus (G). This observation was expected as bond delamination in ISa panels occurred at later

12 stages of the tests in this case.

13 Casacci et al. [15] also investigated the in-plane behavior of unreinforced and strengthened

14 masonry panels using a similar TRM system as strengthening material. The panels were tested at

15 60 days age, and the curing condition of TRM composite was 30 days in the laboratory

16 environmental condition. The maximum shear strength of IU and reinforced wallets (strengthened

17 at both sides) were 0.18 MPa and 0.87 MPa, respectively, while these values for IU and ISa panels

18 tested in the present study are significantly higher (0.6 MPa and 1.78 MPa, respectively). These

19 differences seem to highlight the significant and simultaneous effects of age and curing conditions

20 on the in-plane behavior of panels constructed and strengthened using lime-based mortars.

21 3.6 Out-of-plane test results

22 Fig. 8 shows the load-displacement curves and failure modes of the panels failure parallel (P) and

23 normal (N) to the bed joint under out-of-plane loading. In both unreinforced wallet types (PU and

24 NU), a sudden and brittle failure of masonry after the peak load was observed. In PU, a single

25 crack across the panel and along the bed joint was formed (Fig. 8a), whereas, in NU wallets, the

26 cracks initiated in the head joint and progressed around the units in alternate courses (Fig. 8b).

27 The failure mode of strengthened wallets is also sudden and occurs once the load reaches the tensile

28 strength of the textile, but at a much larger displacement and load capacity, as can be seen in Fig.

29 8a and Fig. 8b. The number of cracks for PS and NS is two and one wide cracks, respectively,

30 formed in the TRM composites at the constant moment region. Like unreinforced wallets, the PS

13

1   wallets failed at the masonry bed joint (Fig. 8a), while the NS wallets failed through the masonry

2   units (Fig. 8b), meaning that the presence of TRM composite did not influence the failure mode

3   of the masonry. In contrast to diagonal compression wallets, no TRM-to-masonry detachment was

4   observed in any of these wallets (with and without sandblasting). This behavior can be due to the

5   differences in the stress states in the system compared to the in-plane tests. The average distance

6   between cracks is 125 mm and 113 mm for PSa and PSb, respectively, slightly larger than the

7   crack spacing observed in TRM tensile tests. This difference can be due to the difference in the

8   load application and boundary conditions in these two test methods.

9   Table 4 reports the main results of the out-of-plane behavior of the wallets tested parallel to the

10 bed joint in terms of the cracking load (P_{cr}) and its corresponding deflection (Δ_{cr}), as well as the

11 maximum load (P_{max}) and its corresponding deflection (Δ_{max}). It can be observed that the

12 application of the glass-based TRM system leads to a significant enhancement of the flexural

13 strength of the panels (37 and 41 times for PSa and PSb, respectively). The deformation capacity

14 of the system is also increased significantly. This parameter can be quantified through the

15 definition of a ductility parameter ($\mu_{bending}$) as follows [19, 47]:

16 $$\mu_{bending} = \frac{1}{2}\left(\frac{E_{max}}{E_{cr}} + 1\right) \dots\dots\dots\dots\dots\dots\dots\dots\dots\dots\dots\dots\dots (4)$$

17 where E_{max} is the area under the load-displacement curve until the maximum load (P_{max}) and E_{cr} is

18 the area until the cracking load (P_{cr}). It can be observed in Table 4 that the $\mu_{bending}$ of PSb wallets

19 (sandblasted wallets) is 1.3 times higher than the ductility of the PSa wallets (wallets with no

20 surface treatment). The role of TRM composite in improving the bending behavior of wallets is

21 also significant in wallets tested normal to the bed joints, see Table 4. The maximum load is 3.3

22 and 2.9 times increased in NSa and NSb, respectively, compared with NU wallets. Sandblasting

23 of the bricks does not show a considerable effect on the out-of-plane behavior. The ductility

24 parameter, however, is higher by 14% in NSb in contrast to NSa.

25 The orthogonal strength ratio (OSR), a parameter about the anisotropy degree of masonry, is equal

26 to the ratio of the gross area modulus of rupture (R) parallel to bed joints (R_P) to that of normal to

27 bed joints (R_N) [18]. According to ASTM E518 [48], R is expressed as follows:

28 $$OSR = \frac{R_P}{R_N}, R = \frac{(P_{max} + 0.75P_s)L_s}{b_m t^2} \dots\dots\dots\dots\dots\dots\dots\dots\dots\dots\dots\dots (5)$$

14

1   in which P_s and L_s are the specimen weight and outer span length (420 mm). b_m and t are

2   corresponding to the width and thickness of the panel (b_m= 420 for PS panels and 330 mm for NS

3   panels). Since wallets are tested in the vertical position, the effect of self-weight on the flexural

4   tensile strength is considered to be zero (P_s= 0). Table 4 shows that the OSR for URM wallets is

5   equal to 9.5, which indicates the URM wallets have a high anisotropy degree. Nevertheless, for

6   the PSa and PSb wallets, it is found to be 1.24 and 0.97, respectively, showing that the TRM

7   composite has a crucial role in significantly decreasing the anisotropy degree.

8   ## 4   Analytical modeling

9   4.1   Crack spacing prediction of TRM composites

10   The ACK-theory is used here to calculate/predict the saturation crack spacing in the tensile

11   specimens. Based on this model, the saturation crack spacing (X) can be obtained by expressing

12   the force equilibrium along the loading axis of the yarns [49, 50]:

13
$$X = 1.337 \frac{\upsilon_m r \, \sigma_{mu}}{\upsilon_f 2\tau_f} \quad\text{..} (6)$$

14   υ_f and υ_m are the volumetric fractions of the yarns, and the mortar, respectively. υ_f is calculated as

15   the ratio between the yarn area mesh and the average cross-section of the specimens (υ_f= 0.00335),

16   while υ_m is equal to 1-υ_f. r is the yarn/cord radius equal to 0.5298 mm for glass yarns (assuming a

17   circular section area). τ_f is the frictional shear strength at the yarn interface and the mortar obtained

18   from the pull-out tests as 2.3 MPa (Table 2). Finally, σ_{mu} is the direct tensile strength of the mortar.

19   In the absence of experimental results, this value can be obtained from the compressive, flexural,

20   or splitting strength [51], as calculated and presented in Table 5. It can be observed that the mortar

21   tensile strength values calculated from these formulations are very similar. Having calculated the

22   τ_f and σ_{mu}, Eq. (6) is used to calculate the saturation crack spacing, see Table 5. It can be observed

23   that the crack spacing is predicted to be around 86~92 mm, which represents a 10~15% error with

24   respect to the experimental results.

25   4.2   Prediction of panels shear strength

26   The shear strength of IU panels can be computed based on the failure mode [16, 19, 52, 53]: the

27   shear sliding, the shear friction, the diagonal tension, and the toe crushing. Since sliding along the

15

1   mortar joint was the failure mode of IU panels, their shear strength (V_{ss}) can be calculated as

2   follows:

3    $$V_{ss} = \frac{\tau_0}{1 - \mu_0 \tan \theta} A_n$$ .... (7)

4   where τ_0 is the shear bond strength obtained from the shear strength of masonry prisms at 28 days

5   (τ_0= 0.26 MPa), and μ_0 is the coefficient of internal shear friction in mortar joint equal to 0.3

6   reported in other studies [16, 19]. Other parameters (θ and A_n) are defined in section 3.5. Therefore,

7   V_{ss} is equal to 20.06 kN, showing a 51% error to the experimental results. This difference can

8   result from the μ_0 value. Paulay and Priestly [54] proposed that μ can vary between 0.3 and 1.2. If

9   μ is equal to 0.66, the V_{ss} will be 41.3 kN equal to the experimental mean value of IU panels.

10   The nominal shear capacity (V_n) of TRM-strengthened panels, based on ACI 549.4R-13 [55],

11   consists of the shear strength provided by the masonry (V_m) and the TRM composites (V_f), as

12   shown in Online Resource 2:

13   $$V_n = V_m + V_f$$ .... (8)

14   Since all strengthened-masonry panels failed under diagonal tension, the masonry shear strength

15   can be calculated as follows:

16   $$V_m = \frac{\tan \theta + \sqrt{21.16 + \tan^2 \theta}}{10.58} f'_t A_n \left(\frac{L}{H_w} \right)$$ .... (9)

17   where f'_t is the tensile strength of masonry and equal to $0.67 \sqrt{f'_m}$, in which f'_m is the compressive

18   strength of masonry (f'_m= 11.1) as reported by [16, 19, 52], and other parameters (θ, A_n, L, and

19   H_w) are defined in section 3.5. Therefore, the masonry shear strength (V_m) is obtained as 65 kN,

20   which is higher than V_{ss} and the experimental result of IU panels due to considering different

21   failure modes.

22   The shear capacity provided by the TRM composites (V_f) can be calculated as [55]:

23   $$V_f = 2nA_f L f_{fv}$$ .... (10)

24   where n and A_f are the number of fabric layers (n= 1) and area of fabric per unit width in both

25   directions (A_f= 0.07054mm^2/mm). f_{fv} is the tensile strength in the TRM reinforcement, which is

26   equal to:

27   $$f_{fv} = E_f \varepsilon_{fv}, \varepsilon_{fv} = \varepsilon_{fu} \le 0.004$$ .... (11)

16

1   where E_f and ε_{fv} are the tensile modulus of elasticity of cracked TRM and the design tensile strain

2   of TRM composites, respectively [55]. Based on ACI 549.4R-13 [55], ε_{fv} should be equal to the

3   ultimate tensile strain of TRM composites ($\varepsilon_{fu}= \varepsilon_3= 0.0119$ from Table 2) and less than 0.004, as

4   presented in Eq. (11). It seems this limitation is because of avoiding large cracks in the TRM

5   composites [56]. By examining the tensile behavior of TRM composite in this study (see Fig. 5

6   and Table 2), it can be seen that ε_{fv} equal to 0.004 occurs precisely at the crack development stage.

7   Having $E_f= 62700$ MPa from the average of the experimental tensile tests (see Table 2) and

8     $\varepsilon_{fv}= 0.004$, f_{fv} can be obtained as 250.8 MPa. Replacing this value in Eq. (10) will lead to a V_f

9   value of 19 kN. Adding Eq. (9) to Eq. (10) will lead to a total shear capacity of the strengthened

10   panels of 84 kN, which is 33% and 44% lower than the experimental results of ISa and ISb panels,

11   respectively (Table 6). This observation is also in agreement with the findings of other studies [16,

12   19, 56]. One possible reason for such a difference between the analytical and experimental results

13   is the erroneous estimation of ε_{fv} in Eq. (11) and the fact that it is limited to 0.004. If ε_{fv} is

14   considered equal to 0.0119, V_f and V_n will be equal to 56.8 kN and 121.8 kN, respectively, which

15   shows a 3% and 19% error to the experimental results ISa and ISb panels, respectively.

16   Another method to determine f_{fv} is combining the results of TRM-to-substrate bond and direct

17   tensile tests performed on the yarn [57]. Such a combination, presented in Fig. 9, allows the

18   calculation of the effective tensile capacity of the textile under more realistic boundary conditions.

19   Here, the average pull-out load-slip curves obtained from samples with 50 mm and 100 mm bond

20   length are also presented and used to calculate this load (values are presented in Table 6). These

21   three values are then used for predicting the TRM shear contribution (V_f) to obtain the total shear

22   capacity, as presented in Table 6. In this method, the error in the prediction of V_n is less (1~21%

23   for ISa panels and 17~34% for the ISb panels, in general). A comparison between the V_f obtained

24   from the single-lap, and pull-out test results show that although SL100-b specimens have a longer

25   bond length than the pull-out specimens with 50 mm embedded length, they are similar tensile

26   capacity and, consequently, V_f can be obtained from them. Also, the pull-out specimens with

27   100 mm embedded length show a higher utilization of tensile capacity than the single-lap samples

28   with the same embedded length because of the difference in the boundary conditions in these two

29   test setups. Overall, it appears that the single-lap test results are more suitable for calculating the

30   tensile capacity of TRM systems due to the more realistic boundary conditions imposed on the

31   samples in this test setup. However, it should also be noted that single-lap shear bond tests

    17

1   represent a specific case where the crack surface is perpendicular to the fabric direction. In reality,

2   the cracks occur at an angle to the fabrics, leading to the involvement of transverse fabric in

3   bidirectional grids. These, which can affect the utilized tensile capacity of the fabrics, are not

4   considered when single-lap shear bond tests are used to calculate f_{fv}.

5   ### 4.3   Prediction of panels flexural strength

6   The nominal flexural strength of unreinforced masonry panels can be calculated as follows [46]:

7    $$M_{Rd} = S f_{xk}$$ ....(12)

8   where S is the section modulus of un-crack wallets (7×10^5 mm^3 and 5.5×10^5 mm^3 for PU and NU

9   panels, respectively). f_{xk} is the flexural strength of masonry and can be calculated based on the

10   masonry unit type and the joint mortar compressive strength [46]. Since the flexural strength of

11   masonry did not measure in this study, f_{xk} is used from what was proposed by EN 1996-1-1 [46].

12   Hence, f_{xk} is equal to 0.1 MPa and 0.4 MPa for PU and NU panels, respectively. Replacing S and

13   f_{xk} in Eq. (12), M_{Rd} can be obtained for PU and NU panels as 0.07 kN.m and 0.22 kN.m,

14   respectively, showing a 22% and 69% error, in contrast to the experimental results. This difference

15   can be due to the estimated flexural strength of masonry (f_{xk}).

16   As for the TRM-strengthened masonry, the nominal flexural strength (M_n) can be calculated

17   following ACI 549.4R-13 [55] formulations:

18    $$M_n = A_f b_m f_{fe} \left(t + \frac{t_c}{2} - \frac{\beta_1 c}{2} \right)$$ ....(13)

$$f_{fe} = E_f \varepsilon_{fe}, \; \varepsilon_{fe} = 0.7 \varepsilon_{fu} \leq 0.012$$

19   where A_f is the fabric area per unit width (A_f= 0.03572 mm^2/mm), and f_{fe} is the effective tensile

20   stress level in the TRM composite. Also, t and t_c, equal to 100 mm and 10 mm, are masonry wallet

21   and TRM composite thicknesses. c is the depth of the effective compressive block (see Online

22   Resource 3), and β_1 is a stress block coefficient equal to 0.7. ε_{fe} is the effective tensile strain level

23   in the TRM, and ε_{fu} is the ultimate tensile strain of TRM composites (Table 2). It should be mention

24   since the masonry compressive strength (f'_m) only was measured perpendicular to the flatwise

25   surface of the brick, f'_m is considered the same value for both PS and NS panels. In Eq. (13), it is

26   assumed that plane sections remain plane after loading, TRM has a linear behavior to failure

27   neglecting its contribution before cracking, and the masonry tensile strength is neglected. Online

28   Resource 3 presents the analytical predictions under both failure directions. M_n is equal to

18

0.80 kN.m and 0.63 kN.m for PS and NS, respectively, lower than the experimental results. Table 6 shows the proportion of M_n to the maximum flexural strength of PS and NS experiments representing a 65~72% error. This observation is also in agreement with the findings of other studies [16, 19, 58].

Based on the approach presented in section 4.2 (the combination of the bond response and the yarn tensile behavior), the effective tensile stress (f_{fe}) level in the TRM composite and the nominal flexural strength (M_n) of PS and NS are presented in Table 6. Combining the pull-out response with 50 mm embedded length and the yarn tensile behavior shows a 70~75% error to the experimental results (see Table 6). The error resulted from the single-lap shear test (SL100-b), and the pull-out response in 100 mm bond length is 67~74% and 47~57%, respectively. It is obvious that all these methods produce a significant error in the prediction of the flexural capacity of TRM-strengthened masonry.

5   Conclusions

A series of multi-level experimental tests were performed to investigate the effect of a glass-based TRM composite and the brick surface treatment on the masonry wallets' behavior. The following main conclusions can be drawn from the experimental results:

- Comparison of the pull-out and debonding (single-lap) shear tests indicated a significant difference in the obtained load-slip curves and failure modes. This difference being significant even when the TRM-to-substrate bond is of high quality (when the surface is treated) due to the differences in the boundary conditions and stress distribution in these two test methods. While pull-out tests provide information for characterization of the fabric-to-mortar bond behavior, debonding tests provide information on the reliability of the strengthening system used.

- Tensile test results showed that curing conditions significantly affected the tensile response in both uncracked and cracked stages, including the cracking strength and saturated crack spacing. As the curing degree of the mortar increases, both cracking strength and saturated crack spacing increase. While the former is favorable, the latter is unfavorable in structural safety.

- The effect of surface preparation on the TRM-to-substrate bond behavior was significant. The sandblasted specimens showed a perfect bond at the TRM-masonry interface, while

19

delamination was observed in the samples prepared with no surface treatment. In both cases, this had a significant influence on the in-plane response of TRM-strengthened panels. However, this influence was less important in out-of-plane tests because of the tension-compression stresses introduced in the TRM system under the test setup boundary conditions.

- Application of one layer of glass-based TRM, used in this study, was observed to significantly influence the in-plane and out-of-plane response of masonry panels. Both the load and deformation capacity increased significantly. The failure mode of the wallets also changed from brittle in URM walls to pseudo-ductile (limited crack development stage followed by brittle failure) in TRM-strengthened masonry.

- Comparing the experimental results obtained in this study with the ones available in the literature that were performed on similar materials showed the significant and simultaneous effect of age and curing conditions on the structural response of strengthened panels. This significant influence is expected to be dependent on the type of mortar used.

- The crack spacing diagonal compression samples were similar to the saturated crack spacing observed in tensile tests. However, the out-of-plane test samples showed a larger crack spacing due to the differences in these samples' stress conditions, which affects the bond behavior as the main controlling mechanism for mortar crack spacing.

- When combined with pull-out tests results, the ACK theory provided satisfactory predictions of the crack spacing in tensile test samples.

- Analytical prediction of the capacity of strengthened panels required calculation of the textile contribution in the load resistance of the whole system. The existing formulations use the tensile capacity of the textile as an input. Single-lap test results seem to be suitable for calculating the effective tensile capacity of TRM systems. However, it should also be noted that single-lap shear bond tests represent a specific case where the crack surface is perpendicular to the fabric direction. In reality, the cracks occur at an angle with respect to the fabrics which can also lead to the involvement of transverse yarns in bidirectional grids. This aspect, which can affect the utilized tensile capacity of the fabrics, is not taken into account and requires further investigation.

20

6 Compliance with ethical standards

Conflict of interest: The authors declare that they have no conflict of interest.

1 # 7   References

2 1. Valvona F, Toti J, Gattulli V, Potenza F (2017) Effective seismic strengthening and
3 monitoring of a masonry vault by using Glass Fiber Reinforced Cementitious Matrix with
4 embedded Fiber Bragg Grating sensors. Compos Part B Eng 113:355–370.
5 https://doi.org/10.1016/j.compositesb.2017.01.024

6 2. Karimi AH, Karimi MS, Kheyroddin A, Shahkarami AA (2016) Experimental and
7 numerical study on seismic behavior of an infilled masonry wall compared to an arched
8 masonry wall. Structures 8:144–153. https://doi.org/10.1016/j.istruc.2016.09.012

9 3. Marques R, Lourenço PB (2019) Structural behaviour and design rules of confined masonry
10 walls: Review and proposals. Constr Build Mater 217:137–155.
11 https://doi.org/10.1016/j.conbuildmat.2019.04.266

12 4. Raoof SM, Koutas LN, Bournas DA (2017) Textile-reinforced mortar (TRM) versus fibre-
13 reinforced polymers (FRP) in flexural strengthening of RC beams. Constr Build Mater
14 151:279–291. https://doi.org/10.1016/j.conbuildmat.2017.05.023

15 5. Trapko T (2013) The effect of high temperature on the performance of CFRP and FRCM
16 confined concrete elements. Compos Part B Eng 54:138–145.
17 https://doi.org/10.1016/j.compositesb.2013.05.016

18 6. Padalu PKVR, Singh Y, Das S (2020) Cyclic two-way out-of-plane testing of unreinforced
19 masonry walls retrofitted using composite materials. Constr Build Mater 238:117784.
20 https://doi.org/10.1016/j.conbuildmat.2019.117784

21 7. De Santis S, de Felice G, Roscini F (2019) Retrofitting of masonry vaults by basalt textile-
22 reinforced mortar overlays. Int J Archit Herit 13:1061–1077.
23 https://doi.org/10.1080/15583058.2019.1597947

24 8. Valluzzi MR, Modena, Claudio V, de Felice G (2014) Current practice and open issues in
25 strengthening historical buildings with composites. Mater Struct 47:1971–1985.
26 https://doi.org/10.1617/s11527-014-0359-7

27 9. D'Antino T, Papanicolaou C (2017) Mechanical characterization of textile reinforced
28 inorganic-matrix composites. Compos Part B Eng 127:.
29 https://doi.org/10.1016/j.compositesb.2017.02.034

30 10. Younis A, Ebead U (2018) Bond characteristics of different FRCM systems. Constr Build
31 Mater 175:610–620. https://doi.org/10.1016/j.conbuildmat.2018.04.216

32 11. Ferretti F, Mazzotti C (2021) FRCM/SRG strengthened masonry in diagonal compression:
33 experimental results and analytical approach proposal. Constr Build Mater 283:122766.
34 https://doi.org/10.1016/j.conbuildmat.2021.122766

35 12. Papanicolaou C, Triantafillou T, Lekka M (2011) Externally bonded grids as strengthening
36 and seismic retrofitting materials of masonry panels. Constr Build Mater 25:504–514.
37 https://doi.org/10.1016/j.conbuildmat.2010.07.018

38 13. Marcari G, Basili M, Vestroni F (2017) Experimental investigation of tuff masonry panels
39 reinforced with surface bonded basalt textile-reinforced mortar. Compos Part B Eng
40 108:131–142. https://doi.org/10.1016/j.compositesb.2016.09.094

41 14. Parisi F, Iovinella I, Balsamo A, et al (2013) In-plane behaviour of tuff masonry
42 strengthened with inorganic matrix-grid composites. Compos Part B Eng 45:.
43 https://doi.org/10.1016/j.compositesb.2012.09.068

44 15. Casacci S, Gentilini C, Di Tommaso A, Oliveira D V. (2019) Shear strengthening of
45 masonry wallettes resorting to structural repointing and FRCM composites. Constr Build

22

Mater 206:19–34. https://doi.org/10.1016/j.conbuildmat.2019.02.044

16. Babaeidarabad S, Arboleda D, Loreto G, Nanni A (2014) Shear strengthening of un-reinforced concrete masonry walls with fabric-reinforced-cementitious-matrix. Constr Build Mater 65:243–253. https://doi.org/10.1016/j.conbuildmat.2014.04.116

17. Wang X, Lam CC, Iu VP (2018) Experimental investigation of in-plane shear behaviour of grey clay brick masonry panels strengthened with SRG. Eng Struct 162:84–96. https://doi.org/10.1016/j.engstruct.2018.02.027

18. Padalu PKVR, Singh Y, Das S (2018) Efficacy of basalt fibre reinforced cement mortar composite for out-of-plane strengthening of unreinforced masonry. Constr Build Mater 191:1172–1190. https://doi.org/10.1016/j.conbuildmat.2018.10.077

19. Sagar SL, Singhal V, Rai DC, Gudur P (2017) Diagonal Shear and Out-of-Plane Flexural Strength of Fabric-Reinforced Cementitious Matrix–Strengthened Masonry Walletes. J Compos Constr 21:. https://doi.org/10.1061/(ASCE)CC.1943-5614.0000796

20. Martins A, Vasconcelos G, Fangueiro R, Cunha F (2015) Experimental assessment of an innovative strengthening material for brick masonry infills. Compos Part B 80:328–342. https://doi.org/10.1016/j.compositesb.2015.06.012

21. Ferrara G, Caggegi C, Martinelli E, Gabor A (2020) Shear capacity of masonry walls externally strengthened using Flax-TRM composite systems : experimental tests and comparative assessment. Constr Build Mater 261:. https://doi.org/10.1016/j.conbuildmat.2020.120490

22. Wang X, Lam CC, Iu VP (2019) Comparison of different types of TRM composites for strengthening masonry panels. Constr Build Mater 219:184–194. https://doi.org/10.1016/j.conbuildmat.2019.05.179

23. Harajli M, Elkhatib H, San-jose JT (2010) Static and cyclic out-of-plane response of masonry walls strengthened using textile-mortar system. J Mater Civ Eng 22:1171–1181. https://doi.org/10.1061/(ASCE)MT.1943-5533.0000128

24. Kariou FA, Triantafyllou SP, Bournas DA, Koutas LN (2018) Out-of-plane response of masonry walls strengthened using textile-mortar system. Constr Build Mater 165:769–781. https://doi.org/10.1016/j.conbuildmat.2018.01.026

25. Basili M, Vestroni F, Marcari G (2019) Brick masonry panels strengthened with textile reinforced mortar: experimentation and numerical analysis. Constr Build Mater 227:117061. https://doi.org/10.1016/j.conbuildmat.2019.117061

26. Shabdin M, Zargaran M, Attari NKA (2018) Experimental diagonal tension (shear) test of Un-Reinforced Masonry (URM) walls strengthened with textile reinforced mortar (TRM). Constr Build Mater 164:704–715. https://doi.org/10.1016/j.conbuildmat.2017.12.234

27. (2005) ASTM C109/C109M-05, Standard test method for compressive strength of hydraulic cement mortars (Using 2-in. or [50-mm] Cube Specimens)

28. (1999) BS EN 1015-11, Methods of test for mortar for masonry. Determination of flexural and compressive strength of hardened mortar

29. (2013) BS EN 12390-13, Testing hardened concrete. Determination of secant modulus of elasticity in compression

30. (2004) ASTM C496/C496M- 04, Standard test method for splitting tensile strength of cylindrical concrete specimens

31. (2005) ASTM C67-05, Standard test methods for smpling and testing brick and structural clay tile

32. (2000) EN 772-1. Methods of test for masonry units – Part 1: Determination of compressive

23

strength

33. (2003) ASTM C1314-03, Standard test method for compressive strength of masonry prisms

34. (2002) BS EN 1052-3, Methods of test for masonry- Part 3: Determination of initial shear strength

35. Dalalbashi A, Ghiassi B, Oliveira DV, Freitas A (2018) Effect of test setup on the fiber-to-mortar pull-out response in TRM composites: experimental and analytical modeling. Compos Part B Eng 143:250–268. https://doi.org/10.1016/j.compositesb.2018.02.010

36. Dalalbashi A, Ghiassi B, Oliveira D V. (2019) Textile-to-mortar bond behaviour in lime-based textile reinforced mortars. Constr Build Mater 227:116682. https://doi.org/10.1016/j.conbuildmat.2019.116682

37. Razavizadeh A, Ghiassi B, Oliveira D V. (2014) Bond behavior of SRG-strengthened masonry units: Testing and numerical modeling. Constr Build Mater 64:387–397. https://doi.org/10.1016/j.conbuildmat.2014.04.070

38. Ghiassi B, Oliveira D V, Marques V, et al (2016) Multi-level characterization of steel reinforced mortars for strengthening of masonry structures. Mater Des 110:903–913. https://doi.org/10.1016/j.matdes.2016.08.034

39. (2002) ASTM E519-02, Standard test method for diagonal tension (shear) in masonry assemblages

40. (1999) BS EN 1052-2, Methods of test for masonry- Part2: Determination of flexural strength.

41. Dalalbashi A, Ghiassi B, Oliveira D V. (2021) Aging of lime-based TRM composites under natural environmental conditions. Constr Build Mater 270:. https://doi.org/10.1016/j.conbuildmat.2020.121853

42. Dalalbashi A, Ghiassi B, Oliveira DV, Freitas A (2018) Fiber-to-mortar bond behavior in TRM composites: effect of embedded length and fiber configuration. Compos Part B Eng 152:43–57. https://doi.org/10.1016/j.compositesb.2018.06.014

43. Mahmood H, Ingham JM (2011) Diagonal compression testing of FRP-retrofitted unreinforced clay brick masonry wallettes. J Compos Constr 15:810–820. https://doi.org/10.1061/(ASCE)CC.1943-5614.0000209

44. Gattesco N, Boem I (2015) Experimental and analytical study to evaluate the effectiveness of an in-plane reinforcement for masonry walls using GFRP meshes. Constr Build Mater 88:94–104. https://doi.org/10.1016/j.conbuildmat.2015.04.014

45. Babaeidarabad S, De Caso F, Nanni A (2014) URM walls strengthened with fabric-reinforced cementitious matrix composite subjected to diagonal compression. J Compos Constr 18:1–9. https://doi.org/10.1061/(ASCE)CC.1943-5614.0000441.

46. European Committee for Standardization EN 1996-1-1: 2005, Eurocode 6- Design of masonry structures- Part 1-1: General rules for reinforced and unreinforced masonry structures

47. Galal K, Sasanian N (2010) Out-of-plane flexural performance of GFRP-reinforced masonry walls. J Compos Constr 14:162–174. https://doi.org/10.1061/(ASCE)CC.1943-5614.0000061

48. (2003) ASTM E518-02, Standard test method for flexural bond strength of masonry

49. Aveston J, Cooper G, Kelly A (1971) Single and multiple fracture, the properties of fibre composites. In: Proceedings of the conference national physical laboratories. London: IPC Science and Technology Press Ltd., pp 15–24

50. Cuypers H, Wastiels J (2006) Stochastic matrix-cracking model for textile reinforced

24

1 cementitious composites under tensile loading. Mater Struct 39:777–786.
2 https://doi.org/10.1617/s11527-005-9053-0
3 51. (2013) fib- International Federation for Structural Concrete. fib Model Code for Concrete
4 Structures 2010
5 52. Li TT., Galati NN., Tumialan JG. G, Nanni A (2005) Analysis of unreinforced masonry
6 concrete walls strengthened with glass fiber-reinforced polymer bars. ACI Struct J 102:569–
7 577
8 53. ACI Committee 440 (2010) ACI 440.7R-10 Guide for design and construction of externally
9 bonded FRP systems for strengthening unreinforced masonry structures
10 54. Paulay T, Priestely MJN (1992) Seismic design of reinforced concrete and masonry
11 buildings. Wiley Interscience
12 55. ACI Committee 549 (2013) ACI 549.4R-13 Design and construction of externally bonded
13 Fabric-Reinforced Cementitious Matrix (FRCM) systems for repair and strengthening
14 concrete and masonry Structures
15 56. Del Zoppo M, Di Ludovico M, Balsamo A, Prota A (2019) Experimental in-plane shear
16 capacity of clay brick masonry panels strengthened with FRCM and FRM composites. J
17 Compos Constr 23:04019038. https://doi.org/10.1061/(ASCE)CC.1943-5614.0000965
18 57. CNR DT 215/2018 (2018) Guide for the design and construction of externally bonded fibre
19 reinforced inorganic matrix systems for strengthening existing structures
20 58. D'Antino T, Carozzi FG, Colombi P, Poggi C (2018) Out-of-plane maximum resisting
21 bending moment of masonry walls strengthened with FRCM composites. Compos Struct
22 202:881–896. https://doi.org/10.1016/j.compstruct.2018.04.054
23
24

8 Supplementary

Online Resource 1. Experimental program.

Objective	Conducted tests	Material	Brick surface	Name
Material characterization test	Compressive test	M1 and M2 mortar, brick	-	-
	Flexural test	M1 and M2 mortar, brick		-
	Elastic modulus test	M1 and M2 mortar, brick		-
	Splitting test	M1 and M2 mortar		-
	Tensile test	glass yarn		-
Textile-to-mortar bond behavior	Single-sided pull-out test	M1 mortar and glass yarn		-
TRM tensile behavior	Tensile test	M1 mortar and glass yarn		-
TRM-to-brick bond behavior	Single-lap shear test	TRM and brick	Original (method a)	SL100-a
			Sandblasted (method b)	SL100-b, SL150-b
In-plane behavior of strengthened masonry	Diagonal compression test	Masonry wallet (URM)	-	IU
		Masonry wallet and TRM	Original (method a)	ISa
			Sandblasted (method b)	ISb
Out-of-plane behavior of strengthened masonry	Bending test, failure parallel and normal to bed joint	Masonry wallet (URM)	-	PU/ NU
		Masonry wallet and TRM	Original (method a)	PSa/ NSa
			Sandblasted (method b)	PSb/ NSb

Online Resource 2. Analytical prediction of shear strength of reinforced panels.

Masonry properties		Masonry contribution (V_m)
Height of the wall [mm]	H_w= 540	
Length of the wall [mm]	L= 540	
Net cross-sectional area [mm²]	A_n= 54000	
Compressive strength of masonry [Mpa]	$f_m^{'} = 11.1$	$V_m = \dfrac{\tan\theta + \sqrt{21.16 + \tan^2\theta}}{10.58} f_t^{'} A_n \left(\dfrac{L}{H_w}\right) =$
Tensile strength of masonry [Mpa]	$f_t^{'} = 0.67\sqrt{f_m^{'}} = 2.23$	$\dfrac{\tan 45 + \sqrt{21.16 + \tan^2 45}}{10.58} 2.23 \times 54000 \left(\dfrac{540}{540}\right) = 65025\,\text{N}$
The inclined angle between the horizontal and main diagonal of the wall	θ= 45°	
TRM properties		**TRM contribution (V_f)**
Area of fabric per unit width in both directions [mm²/mm]	A_f= 2×0.03527= 0.07054	$\varepsilon_{fv} = \varepsilon_{fu} = 0.0119 \nleq 0.004 \Rightarrow \varepsilon_{fv} = 0.004$ $f_{fv} = E_f \varepsilon_{fv} = 62700 \times 0.004 = 250.8\,\text{MPa}$
Ultimate tensile strain of TRM [mm/mm]	ε_{fu}= 0.0119	$V_f = 2nA_f Lf_{fv} = 2 \times 1 \times 0.07054 \times 540 \times 250.8 = 19106\,\text{N}$
Tensile modulus of elasticity of cracked TRM [MPa]	E_f= 62700	**Nominal shear capacity (V_n)**
Number of fabric layers	n= 1	V_n= V_m+ V_f= 65025+ 19106= 84131 N= 84 kN

26

1 Online Resource 3. Analytical prediction of flexural strength of reinforced panels.

Masonry properties	
Thickness of the masonry wallet [mm]	$t = 100$
Width of the masonry wallet considered in the flexural analysis [mm]	$b_m = 420$ and 330 for masonry PS and NS, respectively
Compressive strength of masonry [MPa]	$f'_m = 11.1$
TRM properties	
Area of fabric per unit width [mm^2/mm]	$A_f = 0.03527$
Effective tensile strain level in the TRM [mm/mm]	$\varepsilon_{fe} = 0.7\varepsilon_{fu} = 0.7 \times 0.0119 = 0.0083 \le 0.012 \Rightarrow \varepsilon_{fe} = 0.0083$
Tensile modulus of elasticity of cracked TRM [MPa]	$E_f = 62700$
Thickness of TRM composite [mm]	$t_c = 10$
Flexural strength	
Effective tensile stress level in the TRM composite [MPa]	$f_{fe} = E_f\,\varepsilon_{fe} = 62700 \times 0.0083 = 520.41$
Stress block coefficient related to c	$\beta_1 = 0.7$
Stress block coefficient related to f$_m$	$\gamma = 0.7$
Depth of effective compressive block [mm]	$c = \dfrac{A_f f_{fe}}{\gamma f'_m \beta_1} = \dfrac{0.03527 \times 520.41}{0.7 \times 11.1 \times 0.7} = 3.375$
Nominal flexural strength [N.mm]	$M_n = A_f b_m f_{fe}\left(t + \dfrac{t_c}{2} - \dfrac{\beta_1 c}{2}\right) =$
for PS (failure parallel to bed joint):	$0.03527 \times 420 \times 520.41\left(100 + \dfrac{10}{2} - \dfrac{0.7 \times 3.375}{2}\right) = 800343$
for NS (failure normal to bed joint):	$0.03527 \times 330 \times 520.41\left(100 + \dfrac{10}{2} - \dfrac{0.7 \times 3.375}{2}\right) = 628840$

2

1 Table 1. Mechanical properties of the mortars and the brick.*

Strength [MPa]	Mortar M1		Mortar M2		Brick			Number of specimens for each test material type
	28 days	90 days	28 days	120 days	flatwise	lengthwise	widthwise	
Compressive strength	12.0 (5)	16.8 (11)	5.3 (6)	8.7 (6)	23.5 (5)	22.3 (10)	18.6 (10)	5
Flexural strength	4.7 (8)	4.5 (2)	1.7 (9)	1.7 (9)	4.5 (14)	4.4 (4)	-	5
Splitting tensile strength	0.9 (7)	1.4 (8)	0.3 (11)	0.5 (7)	-	-	-	5
Elastic modulus	6993 (11)	6713 (6)	-	5236 (10)	-	-	9650 (2)	5

2 *CoV of the results is given in percentage inside parentheses.

3

4 Table 2. Mechanical properties of TRM composites.*

Test	P_P [N]	S [mm]	$E_{deb.}$ [N.mm]	$E_{pull.}$ [N.mm]	K [N/mm]	τ_{max} [MPa]	τ_f [MPa]	κ [N/mm³]	β	-	-	Number of specimens
Pull-out (50 mm)	410.3 (12)	0.37 (47)	107.3 (49)	4366.3 (23)	1602.0 (6)	3.2 (13)	2.3 (16)	23.2 (20)	0.0001 (0)	-	-	5
Pull-out (100 mm)	722.5 (7)	1.18 (25)	592.9 (32)	-	2253.3 (37)	-	-	-	-	-	-	5
-	E_1 [GPa]	E_2 [GPa]	E_3 [GPa]	ε_1 [%]	ε_2 [%]	ε_3 [%]	σ_1 [MPa]	σ_2 [MPa]	σ_3 [MPa]	N.C.	D.C. [mm]	-
Tensile	2280.0 (25)	19.4 (28)	62.7 (15)	0.03 (25)	0.68 (30)	1.19 (9)	567.5 (12)	695.0 (5)	995.6 (9)	3 (13)	101 (23)	4
-	P_P [N]	S [mm]	σ [MPa]	K [N/mm]	-	-	-	-	-	-	-	-
Single-lap shear (SL100-a)	237.57 (22)	0.56 (32)	269.43 (22)	461.3 (47)	-	-	-	-	-	-	-	5
Single-lap shear (SL100-b)	507.3 (25)	1.20 (29)	575.4 (25)	975.7 (48)	-	-	-	-	-	-	-	5
Single-lap shear (SL150-b)	729.9 (6)	1.59 (18)	827.8 (6)	445 (28)	-	-	-	-	-	-	-	5

5 *CoV of the results is given in percentage inside parentheses.
6 N.C.: Number of cracks, D.C.: Distance between cracks
7

8

9

10

11

12

13

14

15

16

17 Table 3. Diagonal compression test results. *

28

Specimen	P_{max} [kN]	Failure	τ'_{max} [MPa]	γ_{max} [%]	γ_y [%]	γ_u [%]	$\mu_{diagonal}$	G [MPa]	Number of specimens
IU	41.04 (22)	A & B	0.60 (31)	0.07 (47)	0.04 (40)	0.07 (47)	1.97 (13)	1815 (76)	3
ISa	126.04 (6)	D & A	1.78 (6)	0.09 (2)	0.06 (4)	0.16 (35)	2.74 (37)	2402 (8)	3
ISb	151.01 (0)	E & C	2.20 (1)	0.11 (3)	0.07 (2)	0.24 (1)	3.46 (2)	2488 (1)	2

1 *CoV of the results is given in percentage inside parentheses.
2 A: combined sliding along mortar joint and cracking in the masonry units; B: sliding along mortar joint; C: cracking
3 in the masonry units; D: TRM failure with debonding between TRM and the masonry; E: TRM failure
4
5 Table 4. Flexural test results.*

Specimen	Δ_{cr} [mm]	P_{cr} [kN]	Δ_{max} [mm]	P_{max} [kN]	M_{max} [kN.m]	M_{Rd}/M_{max} [%]	E_{cr} [kN.mm]	E_{max} [kN.mm]	$\mu_{bending}$	R [N/mm²]	OSR	Number of specimens
PU	-	-	1.05 (37)	1 (34)	0.09 (34)	78	-	1 (50)	-	0.15 (34)	9.50	3
PSa	0.48 (15)	24 (6)	3.02 (21)	37 (19)	2.30 (19)	-	7 (11)	85 (33)	7 (35)	3.67 (19)	1.24	3
PSb	0.36 (1)	22 (10)	2.81 (3)	41 (1)	2.58 (1)	-	5 (11)	82 (9)	9 (2)	4.13 (1)	0.97	3
NU	0.26 (51)	10 (21)	1.95 (51)	11 (33)	0.70 (33)	31	2 (72)	20 (71)	7 (57)	1.42 (33)	-	3
NSa	0.20 (18)	27 (7)	1.76 (4)	36 (13)	2.23 (13)	-	4 (25)	47 (12)	7 (10)	4.55 (13)	-	3
NSb	0.18 (13)	28 (13)	1.83 (8)	32 (23)	1.97 (23)	-	3 (29)	46 (15)	8 (16)	4.01 (23)	-	3

6 *CoV of the results is given in percentage inside parentheses.
7
8
9 Table 5. Prediction of saturated crack spacing.

Calculating tensile strength by	σ_{mu} [MPa]	$X_{nom.}$ [mm]	$X_{nom.}/X_{exp.}$ [%]
compressive strength (f_{ck})	$0.3\left(f_{ck}\right)^{2/3} = 0.3\left(16.8\right)^{2/3} = 1.97$	91	90
flexural strength ($f_{ctm.fl}$)	$\dfrac{0.06h_b^{0.7}}{1+0.06h_b^{0.7}}f_{ctm.fl} = \dfrac{0.06\times40^{0.7}}{1+0.06\times40^{0.7}}4.5 = 1.99$	92	91
splitting strength ($f_{ctm,sp}$)	$2.2\left(f_{cm}\right)^{-0.18}f_{ctm,sp} = 2.2\left(16.8\right)^{-0.18}\times1.4 = 1.85$	86	85

10
11
12
13
14
15 Table 6. Prediction of the nominal shear capacity (V_n).

29

Model	f_{fv} [MPa]	V_f [kN]	V_n [kN]	V_n/P_{max} [%]		f_{fe} [MPa]	$M_{n,PS}$ [kN.m]	$M_{n,NS}$ [kN.m]	M_n/M_{max} [%]			
				ISa	ISb				PSa	PSb	NSa	NSb
ACI [55]	250.8	19.1	84.0	67	56	520.4	0.80	0.63	35	31	28	32
Combination of pull-out (50 mm) and tensile behavior	452.5	34.5	99.5	79	66	452.5	0.70	0.55	30	27	25	28
Combination of single-lap (SL100-b) and tensile behavior	486.8	37.1	102.1	81	68	486.8	0.75	0.59	33	29	26	30
Combination of pull-out (100 mm) and tensile behavior	793.3	60.4	125.4	99	83	793.3	1.21	0.95	53	47	43	48

1

2

1

2
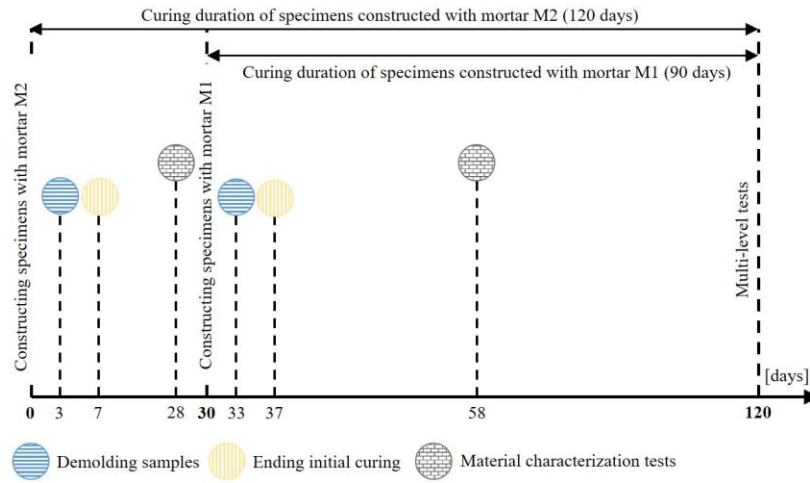
3   Fig. 1. Schematic representation of the test program.

4

31

1

(a)   (b)   (c)
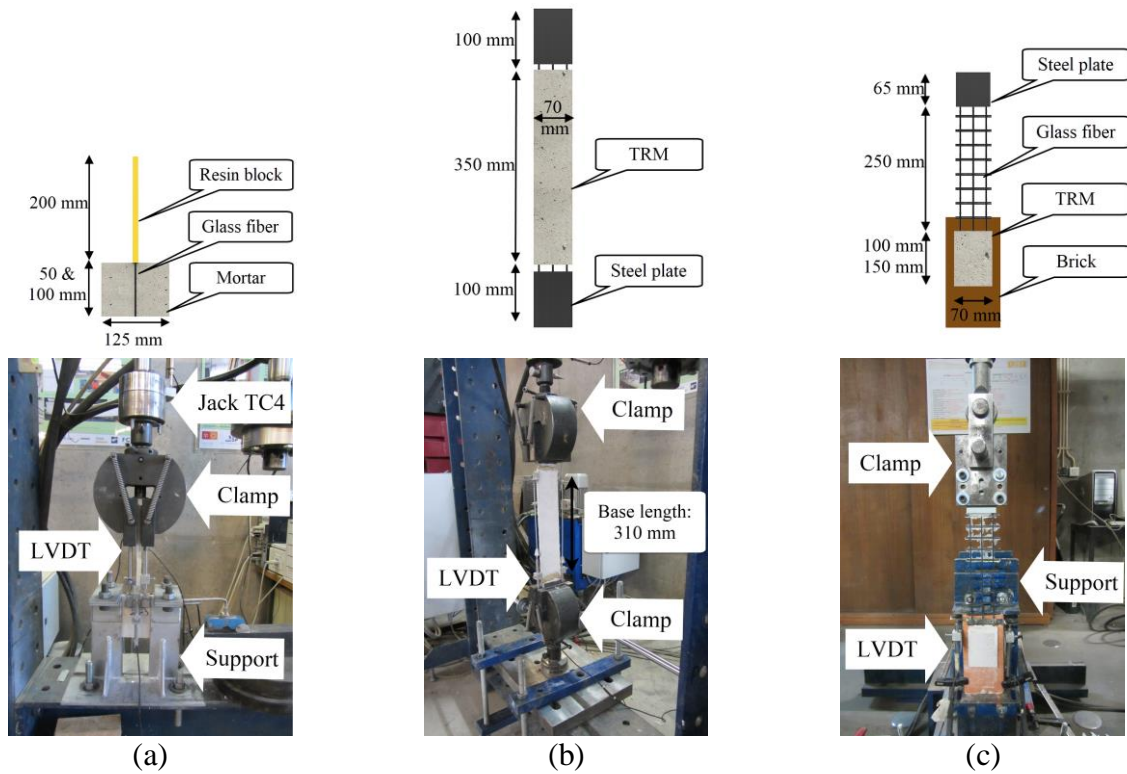
2   Fig. 2. Geometrical and test setups details of the samples: (a) pull-out test; (b) tensile test; (c)
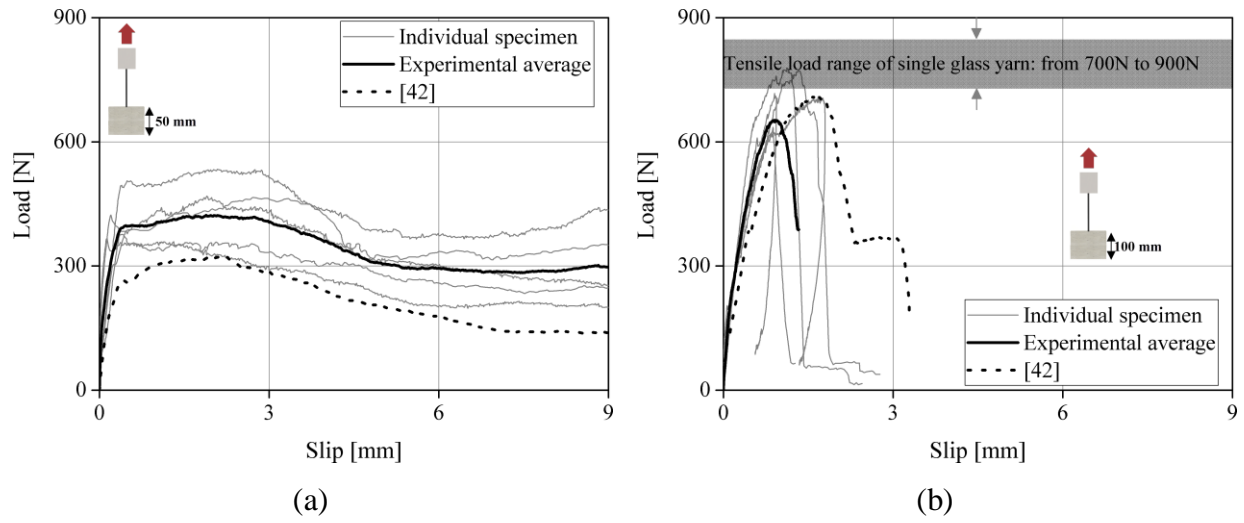
3   single-lap shear test.

4

1

(a) (b) (c)
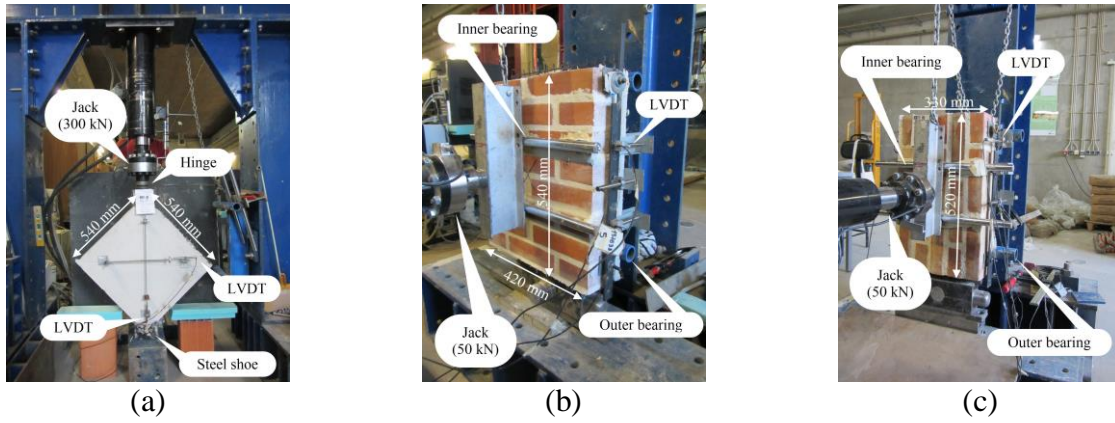
2 Fig. 3. Test setups (a) diagonal compression test; (b) bending test, failure parallel to bed joint; (c)
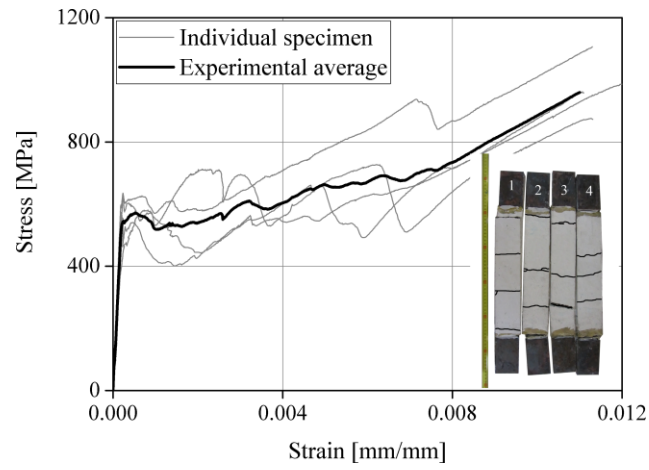3 bending test, failure normal to bed joints.

4

5

1

(a)   (b)

2   Fig. 4. Pull-out response of TRM composite: (a) bond length= 50 mm; (b) bond length= 100 mm.
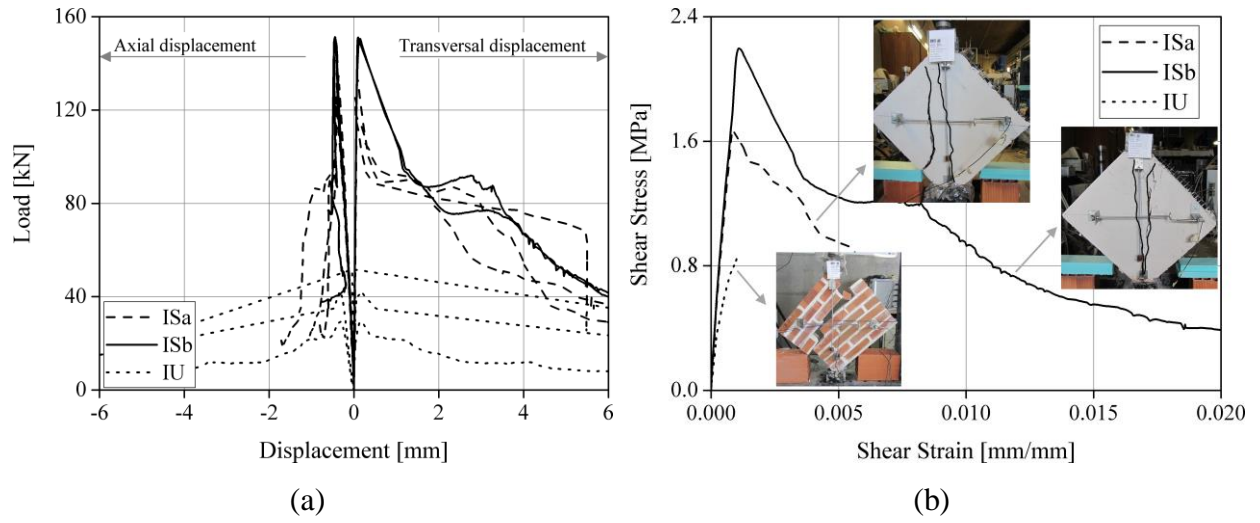
3

4

1

2

3   Fig. 5. Tensile behavior of TRM composite.

4

5

(a)

(b)
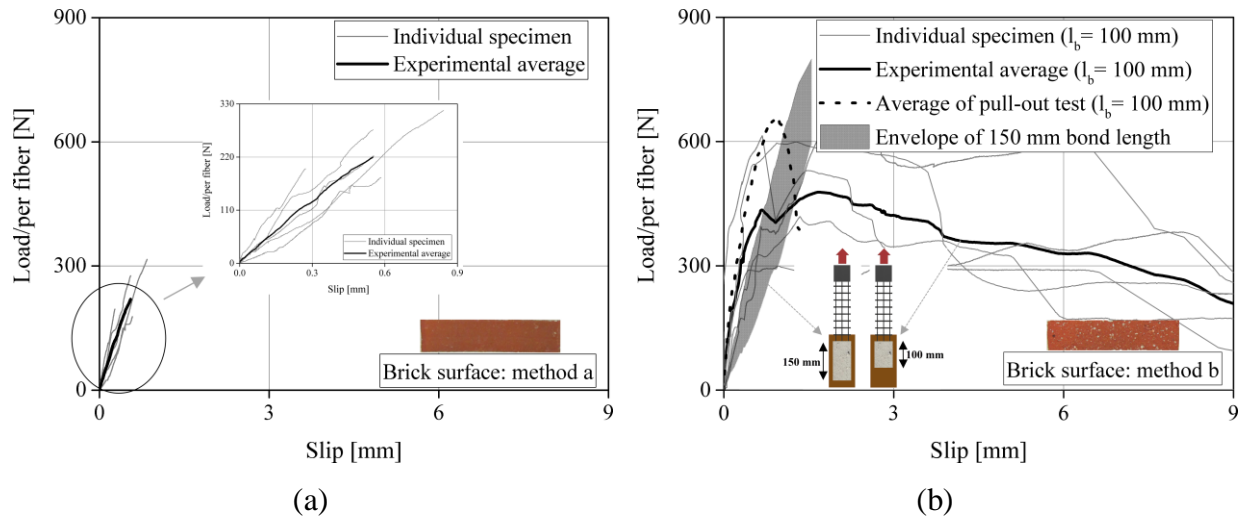
Fig. 6. TRM-to-substrate bond behavior: (a) original brick; (b) sandblasted brick.

1

2

3

(a)

(b)

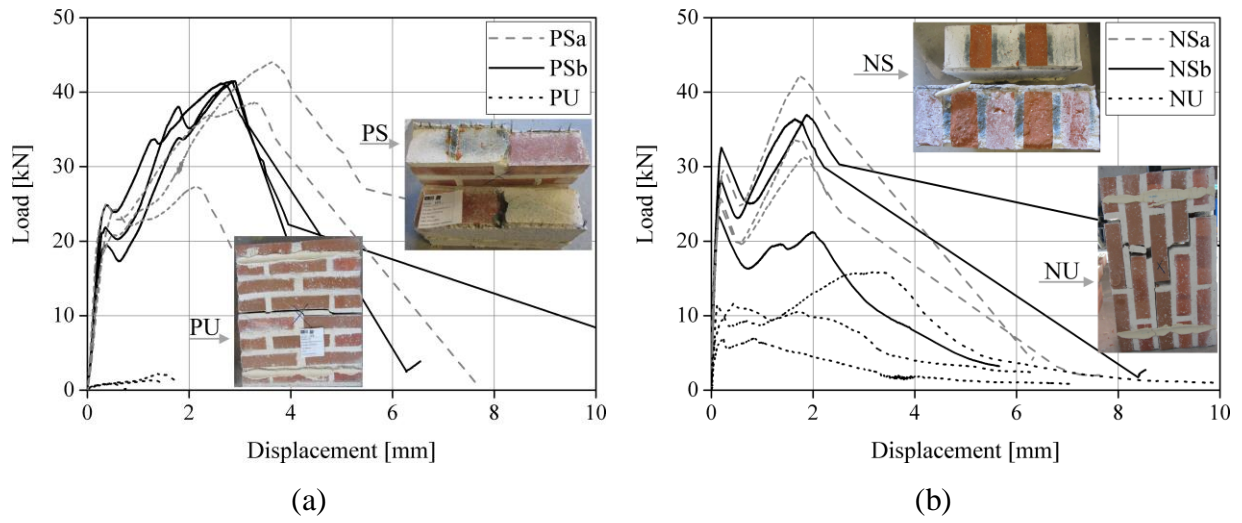Fig. 7. Diagonal compression result: (a) load-displacement curves; (b) average shear stress-strain curves.

1

(a)   (b)
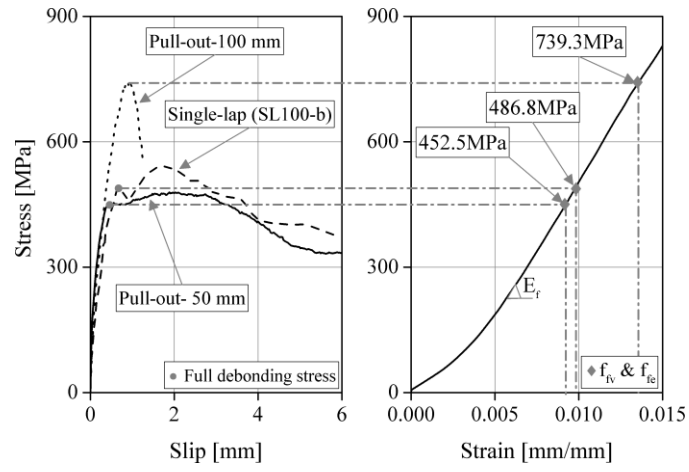
2   Fig. 8. Load-displacement curves of flexural tests: (a) failure parallel to bed joint; (b) failure
3   normal to bed joint.
4

1

2   Fig. 9. Interaction between bond responses and tensile stress-strain of the yarn.

3